Shared Control for the Kinematic and Dynamic Models of a Mobile Robot

Jingjing Jiang, Pierluigi Di Franco, and Alessandro Astolfi, *Fellow, IEEE*

***Abstract*— This paper presents shared-control algorithms for the kinematic and dynamic models of a mobile robot with a feasible configuration set defined by means of linear inequalities. The shared-control laws based on a hysteresis switch are designed in the case in which absolute positions are not available. Instead, we measure the distances to obstacles and angular differences. Formal properties of the closed-loop systems with the shared control are established by a Lyapunov-like analysis. Simulation results and experimental results are presented to show the effectiveness of the algorithm.**

***Index Terms*— Collision avoidance, control constraints, nonlinear control system, robot motion, shared control.**

I. Introduction

MOBILE robots are machines with the ability of locomotion [1]. They are widely used in industry, search and rescue, and military and domestic fields. For instance, mobile robots are used in many warehouses to transfer materials from shelves to loading/unloading areas and vice-versa. Modern troops are equipped with mobile robots for reconnaissance missions and to attack the enemy. We are also able to find domestic robots that perform certain housekeeping tasks, such as vacuuming, window washing, and gardening, being sold on the market. Furthermore, wheelchairs and other assistive devices can also be regarded as mobile robots.

Our study is motivated by the design of smart wheelchairs that are used to help people with mobility disabilities to move safely in their daily life [2]. The shared controller that combines the user input and the feedback control input is installed to reduce the number of accidents and to correct the user's perilous behaviors. Note that the name shared control has the same meaning as that in [3] and as in the antilock braking system. The wheelchair is mostly driven by the operator except for dangerous situations, in which the feedback controller takes charge of the system. It aims to integrate the best of both worlds: the reliable performance of a feedback controller and the adaptive, interactive, and inventive task execution ability of a human operator. Therefore, it is very helpful to the disabled.

Numerous studies and experiments have been performed on mobile robots: we only list here a few of them. Proportional-integral-derivative (PID) controllers are widely used in the industry as well as in the control of mobile robots. Reference [4] has introduced a laser guidance control based on a PD controller to inspect the welds in a nuclear power plant. To avoid collisions, the potential field method is used as discussed in [5], where an attractive force and a repulsive force applied to the robot are generated by the target position and the obstacles, respectively. This may not work well in circumstance in which the combination of a global path generation and a local reactive trajectory generation, based on a focused D* search and an obstacle avoider, respectively, can be used to control the robot [6]. Even though the robot is able to avoid hitting obstacles, it is unable to reach them. Model predictive control (MPC) is another popular method utilized in the design of tracking controller for mobile robots as explained in [7] and [8]. These MPC designs rely on full information on the environment to build the artificial potential and may need large computation for complex environments. H_∞ control and sliding mode control have also been implemented in the control of mobile robots. For instance, [9] has used nonlinear H_∞ control via quasi-linear parameter varying representation to control wheeled robots and [10] has presented an implementation of integral sliding mode controller on a two-wheeled mobile robot. Other control methods, such as back-stepping control [11], adaptive control [12], [13], fuzzy control [14], [15], and control based on the representation as chained system [16]–[18], have also been explored and implemented.

The references introduced in the previous paragraph are on how to design a feedback controller for the automatic navigation of a mobile robot. However, if the human operator is included in the closed-loop system, the situation becomes more complicated. To combine the human input and the feedback control input together, a shared-control algorithm based on the hysteresis switch has been introduced in [19]. Reference [20] has proposed steering-like and brake-like functions according to the distance to the obstacles to avoid collisions, while the human operator drives the robot with a joystick and the stability of the system is analyzed through a linear model. The shared-control problem for a mobile robot has been

Manuscript received October 16, 2015; revised January 25, 2016; accepted January 29, 2016. Date of publication March 18, 2016; date of current version October 14, 2016. Manuscript received in final form February 9, 2016. Recommended by Associate Editor G. Antonelli. *(Corresponding author: Jingjing Jiang.)*

J. Jiang is with the Department of Electrical and Electronic Engineering, Imperial College London, London SW7 2AZ, U.K. (e-mail: jingjing.jiang10@imperial.ac.uk).

P. Di Franco is with the Department of Electrical and Electronic Engineering, Imperial College London, U.K. (e-mail: pierluigi.difranco13@imperial.ac.uk).

A. Astolfi is with the Department of Electrical and Electronic Engineering, Imperial College London, London SW7 2AZ, U.K., and also with the Department of Civil Engineering and Computer Science Engineering, University of Roma Tor Vergata, Rome 00133, Italy (e-mail: a.astolfi@imperial.ac.uk).

Color versions of one or more of the figures in this paper are available online at http://ieeexplore.ieee.org.

Digital Object Identifier 10.1109/TCST.2016.2528890

studied in [21], where the shared controller is used to cope with low-level navigations and thus reduces the operator's workload. However, the human's competence is not improved. Human–robot bilateral shared control has been used in [22], where the robot is able to move autonomously according to the operator's order and a haptic force feedback is available to the human operator indicating the deformation on the desired path. One way to generate the haptic force has been introduced in [23]. Note that high requirements on the human operator are essential for commanding direct motion inputs in a cluttered environment. To reduce the burden of directly driving the robot, [24] has proposed a semiautonomous algorithm at the planning level. Furthermore, a reactive planning approach to bilaterally teleoperate a Unmanned Aerial Vehicle (UAV) has been presented in [25]. Therein the human operator is allowed to modify the path, and an autonomous feedback controller is used to assist the human in reaching the target position. A semiautonomous UAV platform has been presented in [26], in which the haptic feedback reflecting the environment and the system states is available to the human operator. A shared-control law for the kinematic model of a mobile robot with knowledge of the absolute positions is given in [27]. This paper extends the results of [27] to the cases in which absolute positions are not measurable and the shared-control algorithm has to deal with both static and (nonpredefined) dynamic environments. It provides formal proofs of all technical statements, includes additional theoretical results and case studies. Both the simulation results and the experimental ones demonstrate that the robot with the shared controller moves safely without hitting any obstacle. If the feedback controller shares the same objective as the operator, it is used to help the robot safely tracking the trajectory (Cases I and II in Section V). Otherwise, the feedback controller would regard the predicted human behavior as its goal (Case III in Section V).

The rest of this paper is organized as follows. The shared-control problem is formulated in Section II, which also provides a few definitions and assumptions. Novel algorithms to solve the shared-control problem for the kinematic model and the dynamic model of the mobile robot are given in Sections III and IV, respectively. Formal properties of the closed-loop systems with the shared-control algorithm are also established. Section V presents three case studies to illustrate the performance of the shared-control law through simulation and experiments. Finally, conclusions and suggestions for future work are given in Section VI.

II. Problem Formulation, Definitions, and Assumptions

This section formulates the shared-control problem for the kinematic and dynamic models of a unicycle robot. The kinematic model, a simple and common way to study the motion of a wheeled robot, is widely used in the navigation in combination with some low-level controls. It is also the basis of the dynamic model, the control of which is more difficult. However, robots are driven by motors that produce torques, directly relative to the acceleration rather than the velocity of the robots. The dynamic model may be used to describe the situations in which the kinematic model has to be complemented with some additional dynamics, for example, those due to the presence of actuators. Therefore, this paper studies both the kinematic and dynamic models and provides shared-control algorithms for these models.

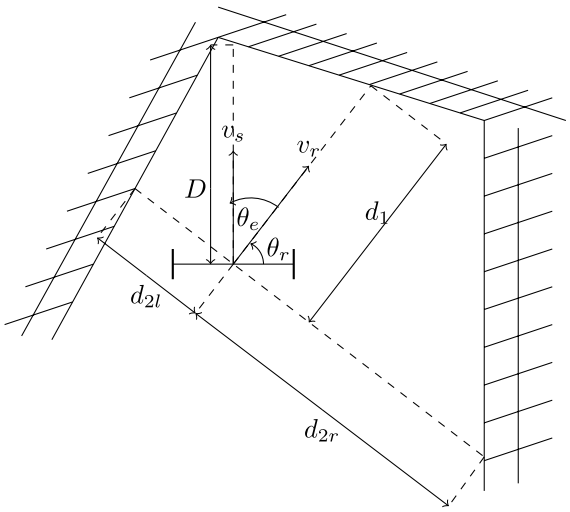

Fig. 1. Definitions of d_1, d_{2l}, d_{2r}, and θ_e (shadowed region: unfeasible region and v_r: reference forward velocity).

The kinematic and dynamic models of a wheeled mobile robot can be described by the equations

$$\begin{aligned} \dot{x} &= v_s \cos\theta \\ \dot{y} &= v_s \sin\theta \\ \dot{\theta} &= \omega_s \end{aligned} \tag{1}$$

and

$$\begin{aligned} \dot{x} &= v \cos\theta \\ \dot{y} &= v \sin\theta \\ \dot{\theta} &= \omega \\ \dot{v} &= u_{1s}/m \\ \dot{\omega} &= u_{2s}/I \end{aligned} \tag{2}$$

respectively, where (x, y) denotes the Cartesian coordinates of the center of mass of the robot, θ denotes the angle between the (positive) heading direction and the x-axis, m and I represent the mass and the moment of the inertia of the robot, respectively. v_s, the linear forward velocity, and ω_s, the angular velocity, are external inputs for system (1), while v and ω are states for system (2), although they still describe the linear forward velocity and the angular velocity, respectively. In addition, u_{1s} and u_{2s} represent the generalized force variable and the steering torque for system (2).

In [27], a shared-control algorithm for a mobile robot with the knowledge of absolute positions has been given. This paper focuses on the shared-control problem without measurement of absolute positions. Instead, the measurements are distances to obstacles along (i.e., d_1) and orthogonal to (i.e., d_2 defined at the end of this paragraph) the direction of v_r and the difference between the real and the reference heading angle (i.e., $\theta_e = \theta - \theta_r$) (see Fig. 1). Note that v_r is

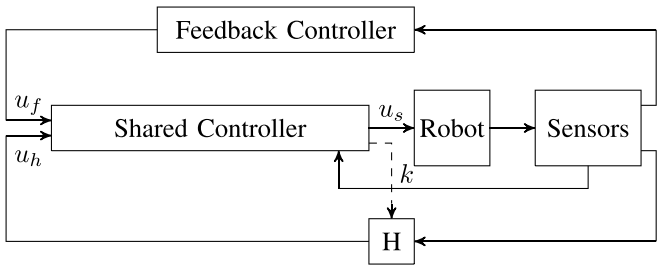

Fig. 2. Proposed control architecture for the closed-loop system with shared control.

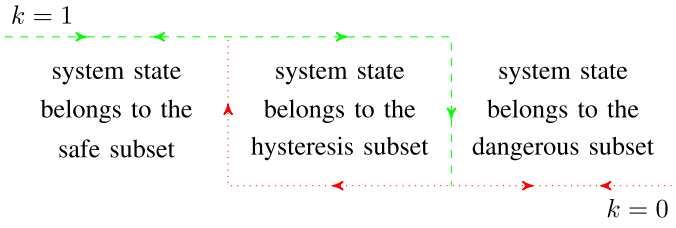

Fig. 3. Sharing function k: $k = 1$ (green dashed line) and $k = 0$ (red dotted line).

the reference linear velocity of the robot. The definition of d_2 is given as

$$d_2 = \begin{cases} d_{2l} & \text{if } \left|\log \dfrac{d_{2l}}{d_{r_{2l}}}\right| \leq \left|\log \dfrac{d_{2r}}{d_{r_{2r}}}\right| \\ d_{2r} & \text{if } \left|\log \dfrac{d_{2l}}{d_{r_{2l}}}\right| > \left|\log \dfrac{d_{2r}}{d_{r_{2r}}}\right| \end{cases} \tag{3}$$

where $d_{r_{2l}}$ and $d_{r_{2r}}$ are defined in what follows in (8).

In the rest of this paper, we use the subscripts h, f, and s to denote the control inputs generated by the human operator, the feedback controller, and the shared controller, respectively.

Definition 1: We use the name *h-control* and *f-control*, denoted by u_h and u_f, to describe the human action and the feedback control action, respectively. In addition, the *sharing function*, denoted by k, is used to quantify how the control authority is shared between u_h and u_f.

The control architecture is given in Fig. 2, where H describes the human action. Note that the function $k \in [0, 1]$ can be used as a feedback signal to the human operator indicating how dangerous the situation is: this is helpful to the human operator in improving his/her behaviors. One possible selection for k is a hysteresis switch, as illustrated in Fig. 3. The overall set describing the feasible values of the state can be divided into three subsets: 1) the safe subset; 2) the hysteresis subset; and 3) the dangerous subset. The variable $k = 1$ if the state belongs to the safe subset or if the state enters the hysteresis subset from the safe subset; $k = 0$ if the state belongs to the dangerous subset or if the state enters the hysteresis subset from the dangerous subset. In addition, as illustrated in Fig. 2, the external input of the mobile robot is the shared-control signal u_s which is a combination of the feedback control input u_f and the human input u_h.

Definition 2: The s-closed-loop and the h-closed-loop for the kinematic model of a mobile robot are used to denote the system described by (1) and

$$\begin{aligned} \dot{x} &= v_h \cos\theta \\ \dot{y} &= v_h \sin\theta \\ \dot{\theta} &= \omega_h \end{aligned}$$

respectively, where v_h and ω_h are the inputs generated by the human operator. Similarly, the s-closed-loop and the h-closed-loop for the dynamic model of a mobile robot are used to denote the system described by (2) and

$$\begin{aligned} \dot{x} &= v \cos\theta \\ \dot{y} &= v \sin\theta \\ \dot{\theta} &= \omega \\ \dot{v} &= u_{1h}/m \\ \dot{\omega} &= u_{2h}/I \end{aligned}$$

respectively, where u_{1h} and u_{2h} are the human inputs. In addition, Ω_h and Ω_s denote the Ω-limit set of h-closed-loop and s-closed-loop, respectively.

Definition 3: The function $f(y(t), x(t), t) = \text{atg}(y(t), x(t), t)$ is a continuous function defined as

$$\text{atg}(y(t), x(t), t) = \text{atan}(y(t), x(t)) + 2\alpha(t)\pi$$

where atan is the four quadrant arctan function, $\alpha(0) = 0$ and

$$\alpha(t) = \begin{cases} \alpha(t - \delta t) + 1, & \text{if } a = -2\pi \\ \alpha(t - \delta t) - 1, & \text{if } a = 2\pi \\ \alpha(t - \delta t), & \text{else} \end{cases}$$

with $a = \lim_{\delta t \to 0^+} \text{atan}(y(t), x(t)) - \text{atan}(y(t - \delta t), x(t - \delta t))$ for all $t > 0$.

Note that Definition 3 is similar to the definition of the standard four quadrant arctan function except that the function atg$(\cdot)$ takes values in $(-\infty, \infty)$ rather than in $[-\pi, \pi)$. The following example can be used to help understand Definition 3. Suppose the robot is tracking a unity circle centered at the origin with the angular speed equals 1, i.e., $x(t) = \cos(t), y(t) = \sin(t)$. Then for any $t \in [0, \pi]$, $\text{atan}(y(t), x(t)) = t$ and $\alpha(t) = 0$. However, $\lim_{\delta t \to 0^+} \text{atan}(y(\pi + \delta t), x(\pi + \delta t)) = -\pi$, indicating that $\lim_{\delta t \to 0^+} \text{atan}(y(\pi + \delta t), x(\pi + \delta t)) - \text{atan}(y(\pi), x(\pi)) = -2\pi$. Therefore, $\alpha(\pi + \delta t) = 1$. It is therefore easy to conclude that, in the example, $\alpha(t) = i$ if $t \in (2i - \pi, 2i + \pi]$, with i a positive integer.

Assumption 1: The admissible Cartesian configuration set for the robot, denoted by $\mathcal{P}_a$, is nonempty.

Assumption 2: The function $d_d(t) = [d_{d1}(t), d_{d2}(t)]^T$, representing the desired distances to the relative obstacles (the obstacles along and orthogonal to the direction of v_r), is continuous.

Assumption 3: To simplify the calculation, we assume that the mass m and the moment of inertia I of the mobile robot are equal to 1.

The above assumptions hold for the rest of this paper.

Suppose $\mathcal{P}_a \subset \mathcal{P} = \mathbb{R}^2$ is a given closed and compact set describing the admissible Cartesian configurations for system (1) and u_h is a given h-control. The shared-control

problem for the kinematic model of a mobile robot can be formulated as follows.

Given system (1), an admissible configuration set $\mathcal{P}_a$, and an h-control, find (if possible) the following:

1) an f-control u_f;
2) a sharing function k;
3) a safe set $\mathcal{R}_s \triangleq \mathcal{P}_a \times \mathcal{A}_s \subset \mathcal{P}_a \times \mathcal{A} \triangleq \mathcal{R}$.

Here, $\mathcal{A}$ and $\mathcal{A}_s$ are the set of all heading angles and the set of all heading angles with which the robot is unable to reach the boundary of $\mathcal{P}_a$ within some arbitrary small time, respectively, such that the s-closed-loop system has the following properties.

P1) The set $\mathcal{R}$ is forward invariant.

P2)

$$\Omega_s = \begin{cases} \Omega_h & \text{if } \Omega_h \subset \mathcal{R}_s \\ \Pi_{\mathcal{R}_s}(\Omega_h) & \text{if } \Omega_h \not\subset \mathcal{R}_s \end{cases}$$

where $\Pi_{\mathcal{R}_s}(\Omega_h)$ is the projection of Ω_h into the set $\mathcal{R}_s$, which will be defined in Section III-A.

P3) $u_s = u_h$ if the state of the s-closed-loop system is in $\mathcal{R}_s$.

Note that the problem statement for the dynamic model (2) is similar to the above one except for that the safe set $\mathcal{R}_s$ is defined as $\mathcal{R}_s \triangleq \mathcal{P}_a \times \mathcal{A}_s \times \mathcal{V}_s \times \mathcal{W} \subset \mathcal{P}_a \times \mathcal{A} \times \mathcal{V} \times \mathcal{W}_f \triangleq \mathcal{R}$ and $\Pi_{\mathcal{R}_s}(\Omega_h)$ will be defined in Section IV-A. $\mathcal{V}$ and $\mathcal{W}$ are the sets of linear velocities and angular velocities, respectively. In addition, for any fixed θ and any $(x, y) \in \mathcal{P}_a$, $\mathcal{V}_s$ and $\mathcal{W}_s$ are the sets of all linear velocities and angular velocities with which the robot is unable to reach the boundary of $\mathcal{P}_a$ within some arbitrary small time, respectively.

III. Shared Control for the Kinematic Model of a Mobile Robot

This section gives a solution to the shared-control problem for the kinematic model of a mobile robot described by (1) with any nonempty $\mathcal{P}_a$.

A. Design of the f-Control

Since measurements of the absolute positions are not available and we can only measure the distances to obstacles and the angular differences between the actual and reference heading angles, the dynamics of system (1) can be rewritten using the variables $d = [d_1, d_2]^T$ and θ_e defined in Section II. If $d_2 = d_{2l}$, then the system controlled by the feedback controller can be described by the equations

$$\begin{aligned} \dot{d}_1 &= -v_f \cos\theta_e \\ \dot{d}_2 &= -v_f \sin\theta_e \\ \dot{\theta}_e &= \omega_f. \end{aligned} \tag{4}$$

Otherwise, if $d_2 = d_{2r}$, then the system controlled with the feedback controller can be described by the equations

$$\begin{aligned} \dot{d}_1 &= -v_f \cos\theta_e \\ \dot{d}_2 &= \ v_f \sin\theta_e \\ \dot{\theta}_e &= \omega_f. \end{aligned} \tag{5}$$

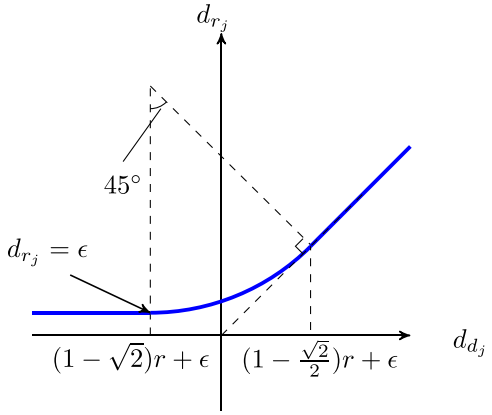

Fig. 4. Graph of the function d_{r_j} given by (8).

Without loss of generality, we only discuss how to design the feedback controller in the case $d_2 = d_{2l}$. Since we regard the mobile robot as a point, the position constraint $(x, y) \in \mathcal{P}_a$ can be rewritten as

$$d_j \geq 0 \quad \forall j \in \{1, 2\}. \tag{6}$$

Define the variable $z = [z_1, z_2]^T$ as

$$z_j = \log \frac{d_j}{d_{r_j}} \tag{7}$$

for all $j \in \{1, 2\}$, where d_{r_j}, describing the reference trajectory for the state d_j, is defined as

$$d_{r_j} = \begin{cases} d_{d_j}, & \text{if } d_{d_j} \geq \left(1 - \dfrac{\sqrt{2}}{2}\right) r + \epsilon \\ \epsilon, & \text{if } d_{d_j} \leq (1-\sqrt{2})r + \epsilon \\ m_j, & \text{otherwise} \end{cases} \tag{8}$$

for all $j \in \{1, 2\}$, with $m_j = (r + \epsilon) - (r^2 - [(\sqrt{2}-1)r - \epsilon + d_{d_j}]^2)^{1/2}$ and a positive constant ϵ. Note that the variable d_{r_j}, instead of d_{d_j}, is used in the definition of z_j, since d_{d_j} may be unfeasible, i.e., there may exist a $t > 0$ such that $d_{d_j}(t) < 0$.

Fig. 4 illustrates the definition of d_{r_j}, from which it is clear that d_{r_j} is a smooth function with positive values. As a result, $\dot{d}_{r_j}$ exists and

$$\dot{d}_{r_1} = -v_r^i, \quad \theta_r = \text{atg}(-d_{r_2}, -d_{r_1}), \quad \dot{\theta}_r = \omega_r. \tag{9}$$

Note that the definition of the safe set $\mathcal{R}_s$ for the system states of the kinematic model of the mobile robot given in Section II is relative to the (x, y) coordinates. However, it can be transferred into the (d_1, d_2, θ) coordinates as follows.

Suppose (d_d, θ_d) is a point of the Ω-limit set of the h-closed-loop system, i.e., $(d_d, \theta_d) \in \Omega_h$, and define the projection of (d_d, θ_d) into $\mathcal{R}_s$ as

$$\Pi_{\mathcal{R}_s}(d_d, \theta_d) = (d_r, \theta_r)$$

where $d_r = [d_{r_1}, d_{r_2}]^T$ and θ_r are defined by (8) and (9), respectively. Then, the projection of Ω_h into the safe set $\mathcal{R}_s$ is defined by

$$\Pi_{\mathcal{R}_s}(d_d, \theta_d) = \{s \in \mathcal{R}_s | s = \Pi_{\mathcal{R}_s}(d_d, \theta_d) \quad \forall (d_d, \theta_d) \in \Omega_h\}.$$

Let $\theta_e^* = \text{atg}(\gamma_2 d_2 z_2, d_1((v_r/d_{r_1}) + \gamma_1 z_1))$, where $\gamma_1 > 0$ and $\gamma_2 > 0$. Note that $\theta_e^*(t)$ is calculated from the backstepping method and it describes the desired value for θ_e at the time instant t. Consider the Lyapunov function relative to $d_2 = d_{2l}$ $L(z_1, z_2, \theta_e)$ given as

$$L(z_1, z_2, \theta_e) = \frac{1}{2}\left[{z_1}^2 + {z_2}^2 + \left(\theta_e - \theta_e^*\right)^2\right] \tag{10}$$

and choose v_f and ω_f such that $\dot{L} < 0$ for all $(z_1, z_2) \neq (0, 0)$ and $\theta_e \neq \theta_e^*$. One such a choice is given by

$$\begin{aligned} v_f &= \sqrt{{d_1}^2\left(\frac{v_r}{d_{r_1}} + \gamma_1 z_1\right)^2 + \gamma_2^2 {d_2}^2 {z_2}^2} \\ \omega_f &= \dot{\theta}_e^* - \gamma_3\left(\theta_e - \theta_e^*\right) - \frac{z_1 v_f \sin\frac{\theta_e + \theta_e^*}{2}\text{sinc}\frac{\theta_e - \theta_e^*}{2}}{d_1} \\ &\quad + \omega_r + \frac{z_2 v_f \cos\frac{\theta_e + \theta_e^*}{2}\text{sinc}\frac{\theta_e - \theta_e^*}{2}}{d_2} \end{aligned}$$

yielding

$$\dot{L} = -\gamma_1 {z_1}^2 - \gamma_2 {z_2}^2 - \gamma_3\left(\theta_e - \theta_e^*\right)^2 \leq 0.$$

This can be pushed back to the (d_1, d_2, θ_e) coordinates yielding

$$\begin{aligned} v_f &= \sqrt{{d_1}^2\left(\frac{v_r}{d_{r_1}} + \gamma_1 \log\frac{d_1}{d_{r_1}}\right)^2 + \gamma_2^2 {d_2}^2\left(\log\frac{d_2}{d_{r_2}}\right)^2} \\ \omega_f &= -\frac{\log\frac{d_1}{d_{r_1}} v_f \sin\frac{\theta_e + \theta_e^*}{2}\text{sinc}\frac{\theta_e - \theta_e^*}{2}}{d_1} \\ &\quad + \frac{\log\frac{d_2}{d_{r_2}} v_f \cos\frac{\theta_e + \theta_e^*}{2}\text{sinc}\frac{\theta_e - \theta_e^*}{2}}{d_2} \\ &\quad + \dot{\theta}_e^* - \gamma_3\left(\theta_e - \theta_e^*\right) + \omega_r \end{aligned} \tag{11}$$

where

$$\theta_e^* = \text{atg}\left(\gamma_2 d_2 \log\frac{d_2}{d_{r_2}}, d_1\left(\frac{v_r}{d_{r_1}} + \gamma_1 \log\frac{d_1}{d_{r_1}}\right)\right).$$

We are now ready to present a preliminary result.

Lemma 1: Consider the f-closed-loop system (1) with $[v_s, \omega_s]^T = [v_f, \omega_f]^T, d_r$ and (v_r, ω_r) given by (11), (8), and (9), respectively. Assume that $(x(0), y(0)) \in \mathcal{P}_a$. Then, the closed-loop system has the following properties.

1) $d_1(t) > 0$, $d_2(t) > 0$ for all $t \geq 0$.
2) $\lim_{t\to\infty}(d_1(t) - d_{r_1}(t)) = \lim_{t\to\infty}(d_2(t) - d_{r_2}(t)) = 0$.

Proof: According to the definition of z_j given in (7), $d_j(t) > 0$ for all $t \geq 0$ and $j \in \{1, 2\}$. The first claim thus holds.

Consider the Lyapunov function (10) and note that $\dot{L}(t) < 0$ for all $z \neq 0$ and $\theta_e \neq 0$. As a result, z and θ_e asymptotically converge to 0 and θ_r, respectively, which proves the second property. ■

B. Shared Control

For any given human input v_h, the safe, hysteresis, and dangerous subsets, $\mathcal{R}_s, \mathcal{R}_h$, and $\mathcal{R}_d$, are defined in (12), as shown at the bottom of this page, where D is the distance to the obstacle along the direction of v_h (see Fig. 1) and $b_2 > b_1 > 0$ are user selected parameters. The three subsets have the following properties.

1) For any fixed v_h, the union of the safe, the hysteresis, and the dangerous set coincides with the overall feasible state space, i.e., $\mathcal{R}_s(v_h) \cup \mathcal{R}_h(v_h) \cup \mathcal{R}_d(v_h) = \mathcal{R}(v_h)$.
2) For any fixed v_h, there is no intersection between the safe subset and the dangerous subset, i.e., $\mathcal{R}_s(v_h) \cap \mathcal{R}_d(v_h) = \emptyset$.

For each group of constraints, the sharing function k can be defined as (see [28])

$$k(D, v_h) = \begin{cases} 1, & (d_1, d_2, \theta_e) \in \mathcal{R}_s(v_h) \\ l, & (d_1, d_2, \theta_e) \in \mathcal{R}_h(v_h) \\ 0, & (d_1, d_2, \theta_e) \in \mathcal{R}_d(v_h) \end{cases} \tag{13}$$

where

$$l = \begin{cases} 1, & \text{if } (d_1, d_2, \theta_e) \text{ enters } \mathcal{R}_h(v_h) \text{ from } \mathcal{R}_s(v_h) \\ 0, & \text{if } (d_1, d_2, \theta_e) \text{ enters } \mathcal{R}_h(v_h) \text{ from } \mathcal{R}_d(v_h). \end{cases}$$

Finally, the overall shared control for system (4) is given by

$$u_s = (1 - k(D, v_h))u_f(d, d_r, \theta_r, \omega_r, v_r) + k(D, v_h)u_h. \tag{14}$$

Theorem 1: Consider the kinematic model of a mobile robot (1) with the shared-control law given by (11)–(14). Assume that $p(0) = [x(0), y(0)]^T \in \mathcal{P}_a$ and u_h is a given h-control. Then, there exist $\gamma_i > 0$, for all $i \in \{1, 2\}$ and $b_2 > b_1 > 0$ such that the s-closed-loop system has the following properties.

1) $p(t)$ stays in $\mathcal{P}_a$ for all $t \geq 0$.
2) $\Omega_s = \Pi_{\mathcal{R}_s}(\Omega_h)$.
3) $u_s(t) = u_h(t)$ if the system state belongs to the safe subset at time t.
4) The feedback-control input u_f is bounded.

$$\begin{aligned} \mathcal{R}_s(v_h) &= \left\{(d_1, d_2, \theta_e + \theta_r) \in \mathbb{R}^+ \times \mathbb{R}^+ \times \mathbb{S} : v_h \leq \frac{1}{b_2 - D} - \frac{1}{b_2} \quad \text{if } D \leq b_2\right\} \\ \mathcal{R}_h(v_h) &= \left\{\begin{array}{l} (d_1, d_2, \theta_e + \theta_r) \in \mathbb{R}^+ \times \mathbb{R}^+ \times \mathbb{S} : \dfrac{1}{b_2 - D} - \dfrac{1}{b_2} < v_h < \dfrac{1}{b_1 - D} - \dfrac{1}{b_1} \text{ and } D \leq b_1 \\ \qquad\qquad \text{or } v_h > \dfrac{1}{b_2 - D} - \dfrac{1}{b_2} \text{ and } b_1 \leq D \leq b_2 \end{array}\right\} \\ \mathcal{R}_d(v_h) &= \left\{(d_1, d_2, \theta_e + \theta_r) \in \mathbb{R}^+ \times \mathbb{R}^+ \times \mathbb{S} : v_h \geq \frac{1}{b_1 - D} - \frac{1}{b_1} \text{ and } 0 \leq D \leq b_1\right\} \end{aligned} \tag{12}$$

Proof: To begin with, as detailed in Section III-A, the f-control u_f is such that the configuration of the system stays in the admissible region $\mathcal{P}_a$. Consider the Lyapunov function candidate L given by (10). Due to the definition of d_2 given in (3), the switch from $d_2 = d_{2l}$ to $d_2 = d_{2r}$ (or vice versa) does not cause any discontinuity in the value of it. If u_s does not switch from one feedback controller to the other, i.e., if (d_1, d_2, θ) leaves the dangerous subset $\mathcal{R}_d$ at $t = t_1$ and enters it again at $t = t_2$, then due to the existence of the hysteresis subset, there exists a positive δt such that $u_s(t) = u_f(t)$ for all $t \in [t_1, t_1 + \delta t]$. Let Δt be the smallest time period, in which one of the feedback controllers is active. Note that $\Delta t > 0$. Then, it is always possible to find positive constants γ_1, γ_2, and γ_3 such that

$$\int_{t_2}^{t_2+\Delta t} \dot{L} dt \leq L(t_1) - L(t_2)$$

that is, $L(t_2 + \Delta t) \leq L(t_1)$. Let $u_f^{i_1}, u_f^{i_2}, \ldots, u_f^{i_n}$ be a series of active feedback controllers and let $u_f^{i_j}$ be active for the time interval $(t_{i_j}, T_{i_j}]$, where $i_j \in \{1, 2, \ldots, i_n\}$ for all $j \in \{1, 2, \ldots, n\}$. Note that $t_{i_{j+1}} \geq T_{i_j}$ for all $j \in \{1, 2, \ldots, n-1\}$. Therefore, $0 \leq L^{i_n}(T_{i_n}) \leq \cdots \leq L^{i_2}(T_{i_2}) \leq L^{i_1}(T_{i_1})$. Define the overall Lyapunov function $L(t)$ as

$$L(t) = L^{i_j}(t), \quad \text{if } t \in (t_{i_j}, T_{i_j}].$$

From the above analysis and [29], $L(t)$ is a multiple Lyapunov function and this implies that the configuration of the system with the feedback controller stays in the admissible set for all $t \geq 0$. In addition, the definition of $\mathcal{R}_d$ indicates that any trajectory enters the dangerous subset $\mathcal{R}_d$ before leaving $\mathcal{R}$, where u_f is active. Therefore, the set $\mathcal{R}$ is a forward invariant set and claim i) holds.

If $\mathbf{\Omega}_h \subset \mathcal{R}_s$, then claim ii) is a consequence of the general results in [28], and of the fact that $\mathbf{\Omega}_h$ is the $\mathbf{\Omega}$-limit set of both the h-closed-loop and f-closed-loop systems [by assumption, the former, and by (7)–(10), the latter]. Otherwise, if $\mathbf{\Omega}_h \not\subset \mathcal{R}_s$, Lemma 1 indicates that the $\mathbf{\Omega}$-limit set of the f-closed-loop system is $\Pi_{\mathcal{R}_s}(\mathbf{\Omega}_h)$. Furthermore, (12) indicates that the trajectory of the system enters $\mathcal{R}_d$, where the feedback controller is active, hence driving the states of the system back to $\mathcal{R}_s$, before leaving the admissible set $\mathcal{R}$. Therefore, property ii) holds.

Statement iii) is a direct consequence of the definition of u_s.

Finally, u_f given by (11) is chosen such that z and θ_e asymptotically converge to zero. Therefore, z is bounded. In addition, $d_{r_j}(t)$ given by (8) for $j \in \{1, 2\}$ is a function with all positive values. This leads to the result $d(t) \geq \epsilon$ for all $t \geq 0$ and some positive constant ϵ. Hence, u_f is bounded. ∎

Note that the third property in Theorem 1 is essential if the shared controller is applied to a training system, such as a training wheelchair. In addition, this property allows the human operator to do whatever he/she wants as long as his/her behavior is safe. This is important, for example, in the application to toy cars.

IV. Shared Control for the Dynamic Model of a Mobile Robot

In this section, we discuss how to design a shared controller for the dynamic model of the mobile robot satisfying all the properties presented in Section II with any nonempty admissible configuration set.

A. Design of the f-Control

Consistently with Section III-A, we design the feedback controller for the case $d_2 = d_{2l}$. Define variables z and d_r as in (7) and (8), respectively. Then, system (2) with the variable z and θ_e can be rewritten as

$$\begin{aligned}
\dot{z}_1 &= \frac{\dot{d}_1}{d_1} - \frac{\dot{d}_{r_1}}{d_{r_1}} = \frac{v_r}{d_{r_1}} - \frac{v\cos\theta_e}{d_1} \\
\dot{z}_2 &= \frac{\dot{d}_2}{d_2} - \frac{\dot{d}_{r_2}}{d_{r_2}} = -\frac{v\sin\theta_e}{d_2} \\
\dot{\theta}_e &= \omega_e \\
\dot{v} &= u_{1f} \\
\dot{\omega}_e &= u_{2f} - u_{2r}
\end{aligned}$$

where $u_r = [u_{1r}, u_{2r}]^T$ is the reference input signal and it is calculated as

$$u_{1r} = \ddot{d}_{r_1}, \quad u_{2r} = \ddot{\theta}_r. \tag{15}$$

Similarly to what stated in Section III-A, even though the definition of the safe set $\mathcal{R}_s$ for the states of the dynamic model of the mobile robot is given based on the (x, y) coordinates, it can be mapped into the $(d_1, d_2, \theta, v, \omega)$ coordinates. Suppose $(d_d, \theta_d, v_d, \omega_d)$ is a point of the $\mathbf{\Omega}$-limit set of the h-closed-loop system, i.e., $(d_d, \theta_d, v_d, \omega_d) \in \mathbf{\Omega}_h$, and define the projection of $(d_d, \theta_d, v_d, \omega_d)$ into $\mathcal{R}_s$ as

$$\Pi_{\mathcal{R}_s}(d_d, \theta_d, v_d, \omega_d) = (d_r, \theta_r, v_r, \omega_r)$$

where d_r and θ_r, v_r, ω_r are defined as in (8) and (9), respectively. Then the projection of $\mathbf{\Omega}_h$ into the safe set $\mathcal{R}_s$ is defined by

$$\Pi_{\mathcal{R}_s}(d_d, \theta_d, v_d, \omega_d) = \left\{ s \in \mathcal{R}_s \;\middle|\; \begin{matrix} s = \Pi_{\mathcal{R}_s}(d_d, \theta_d, v_d, \omega_d) \\ \forall (d_d, \theta_d, v_d, \omega_d) \in \mathbf{\Omega}_h \end{matrix} \right\}.$$

Let

$$\begin{aligned}
\theta_e^* &= \operatorname{atg}\left(\gamma_2 d_2 z_2, d_1\left(\frac{v_r}{d_{r_1}} + \gamma_1 z_1\right)\right) \\
v^* &= \sqrt{(d_1\left(\frac{v_r}{d_{r_1}}\right) + \gamma_1 z_1)^2 + (\gamma_2 d_2 z_2)^2} \\
\omega_e^* &= \dot{\theta}_e^* - \frac{z_1 v^*}{d_1}\sin\frac{\theta_e + \theta_e^*}{2}\operatorname{sinc}\frac{\theta_e^i - \theta_e^*}{2} \\
&\quad + \frac{z_2^i v^*}{d_2}\cos\frac{\theta_e + \theta_e^*}{2}\operatorname{sinc}\frac{\theta_e - \theta_e^*}{2}
\end{aligned}$$

where $\gamma_1 > 0$ and $\gamma_2 > 0$. Consider the Lypunov function

$$L(z_1, z_2, \theta_e, v, \omega_e) = \frac{1}{2}\begin{bmatrix} z_1^2 + z_2^2 + \left(\theta_e - \theta_e^*\right)^2 + (v - v^*)^2 \\ +\left(\omega_e - \omega_e^*\right)^2 \end{bmatrix} \tag{16}$$

and choose $u_f = [u_{1f}, u_{2f}]^T$ such that $\dot{L} \leq 0$ and $\dot{L} \equiv 0$ implies that $(z_1, z_2, \theta_e, v, \omega_e) = (0, 0, 0, 0, 0)$. One such a choice is given by

$$u_{1f} = \dot{v}^* + \frac{z_1}{d_1}\cos\theta_e^i + \frac{z_2}{d_2}\sin\theta_e - \gamma_3(v - v^*)$$
$$u_{2f} = u_{2r} + \dot{\omega}_e^* - \theta_e + \theta_e^* - \gamma_4(\omega_e - \omega_e^*)$$

yielding

$$\dot{L} = -\gamma_1 {z_1}^2 - \gamma_2 {z_2}^2 - \gamma_3(v - v^*)^2 - \gamma_4(\omega_e - \omega_e^*)^2.$$

This can be pushed back into the $(d_1, d_2, \theta_e, v, \omega_e)$ coordinates yielding

$$u_{1f} = \dot{v}^* + \frac{\log\frac{d_1}{d_{r1}}}{d_1}\cos\theta_e + \frac{\log\frac{d_2}{d_{r2}}}{d_2}\sin\theta_e - \gamma_3(v - v^*)$$
$$u_{2f} = u_{2r} + \dot{\omega}_e^* - \theta_e + \theta_e^* - \gamma_4(\omega_e - \omega_e^*) \quad (17)$$

where

$$\theta_e^* = \text{atg}\left(\gamma_2 d_2 \log\frac{d_2}{d_{r_2}}, d_1\left(\frac{v_r}{d_{r_1}} + \gamma_1 \log\frac{d_1}{d_{r_1}}\right)\right)$$

$$v^* = \sqrt{\left(d_1\left(\frac{v_r}{d_{r_1}}\right) + \gamma_1 \log\frac{d_1}{d_{r_1}}\right)^2 + \left(\gamma_2 d_2 \log\frac{d_2}{d_{r_2}}\right)^2}$$

$$\omega_e^* = \dot{\theta}_e^* - \frac{\log\frac{d_1}{d_{r_1}}v^*}{d_1}\sin\frac{\theta_e + \theta_e^*}{2}\text{sinc}\frac{\theta_e - \theta_e^*}{2}$$
$$+ \frac{\log\frac{d_2}{d_{r_2}}v^*}{d_2}\cos\frac{\theta_e + \theta_e^*}{2}\text{sinc}\frac{\theta_e - \theta_e^*}{2}.$$

Lemma 2: Consider the f-closed-loop system (2) with $[v_s, \omega_s]^T = [u_{1f}, u_{2f}]^T, d_r$, and (v_r, ω_r) given by (17), (8), and (9), respectively. Assume that $(x(0), y(0)) \in \mathcal{P}_a$. Then, the closed-loop system has the following properties.

1) $d_1(t) > 0$, $d_2(t) > 0$ for all $t \geq 0$.
2) $\lim_{t\to\infty}(d_1(t) - d_{r_1}(t)) = \lim_{t\to\infty}(d_2(t) - d_{r_2}(t)) = 0$.

B. Shared Control

The definitions of the three subsets, the safe subset $\mathcal{R}_s$, the hysteresis subset $\mathcal{R}_h$, and the dangerous subset $\mathcal{R}_d$, are similar to that given in (12) except for that these three subsets are sets in $(d_1, d_2, \theta_e + \theta_r, v, \omega_e + \omega_r) \in \mathbb{R}^+ \times \mathbb{R}^+ \times \mathbb{S} \times \mathbb{R}^2$. In addition, the sharing function k_d can be defined as in (13). Therefore, the overall shared control for system (2) is given, similar to (14), by

$$u_s = (1 - k_d(D, v_h))u_f(d, d_r, \theta_e, v, \omega_e\theta_r, \omega_r, v_r, u_r)$$
$$+ k_d(D, v_h)\ u_h. \quad (18)$$

Theorem 2: Consider the dynamic model of the mobile robot (2) with the shared-control law given by (13)–(18). Assume that $p(0) = [x(0), y(0)]^T \in \mathcal{P}_a$ and u_h is a given h-control. Then, there exist $\gamma_i > 0$, for all $i \in \{1, 2, 3, 4\}$ and $b_2 > b_1 > 0$ such that the s-closed-loop system has Properties i)–iv) in Theorem 1.

Proof: The proof is similar to that of Theorem 1, hence it is omitted. ■

Fig. 5. Experimental setup.

Remark 1: According to the shared-control law (12)–(14) and (12)–(18) for the kinematic and dynamic models of the mobile robot, the feedback controller is active only if the robot is close to an obstacle. Therefore, d_j can be modified by $\hat{d}_j = \min(d_j, \mathcal{B})$, for $j \in \{1, 2\}$, where $\mathcal{B}$ is a positive constant selected by the user.

Remark 1 indicates that we are not interested in the cases in which $d_j > \mathcal{B}$. This is very useful in applications, especially in the cases in which the obstacle is exactly parallel or perpendicular to the required direction, i.e., d_1 or d_2 equals infinity.

V. Case Studies

In this section, we discuss three case studies: trajectory tracking in a static environment and a dynamic environment, and free-driving. In the first case the human is asked to drive the robot along a given trajectory from the initial position to a final target position in a static rectangular room, while in the second case a person is walking across the room. Finally, in the third case, no task has been given to the operator and he/she plays freely with the robot. By comparing the simulation results and the experimental ones for the first and second case studies, we demonstrate that the trajectory for the robot in the experiment is close to that simulated, indicating the usefulness of the simulation. We provide only experimental results for the third case study. Note that we have only used the kinematic controller in the experiment because the robots available in the laboratory are all controlled directly by velocities.

Both experiments are performed with a Pioneer 3-AT robot with the help of a robotic operative system named as Pioneer 2 Operative System (P2OS). We have used Inertial Measurement Unit (IMU) to measure the angles, angular speed, and magnetic field and lasers together with a Madgwick filter to measure the distances. Sixteen sonars (rate =25 Hz, detection range ≈20°) are used in the experiments, their positions are fixed facing outward with 20° intervals. To estimate the positions, an extended Kalman filter has been used to combine the encoder data (which is inaccurate in long time) and the IMU data. In addition, the human input has been generated by the joystick controller placed on the top of the computer in Fig. 5. The overall system is illustrated in Fig. 5. The projection of the robot in the

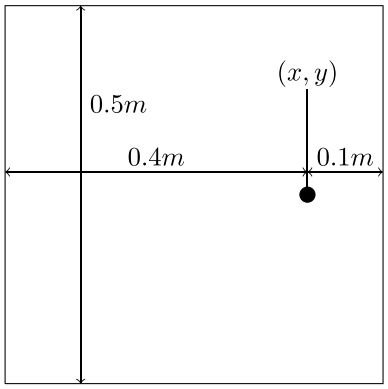

Fig. 6. Projection of the robot in the (x, y)-plane. Round mark: the sensor fixed on the robot. The right edge and the left edge of the square represent the front edge and the back edge of the robot, respectively.

(x, y)-plane is a square with a side length of 0.5 m × 0.5 m. We assume that the sensors are fixed to the middle of the two front-wheels and Fig. 6 illustrates how the robot looks like in the (x, y)-plane.

The Mobilerobot platform uses a client–server mobile robot control architecture managed by the P2OS to insulate the developers from the lowest level of the motor control. In fact, it uses a PID controller with wheel encoder feedback to adjust a pulsewidth modulated signal at the motor driver to control the power to the motors. It has been found that a fully loaded robot works best with $K_p = 85$, $K_v = 86$, $K_i = 87$ and $K_p = 82$, $K_v = 83$, $K_i = 84$ for the translation and rotation movement, respectively. To set up the experiment, we choose the sampling time to be 0.1 s. The distance to the obstacle is calculated as $d = (ct)/2$, where c is the sound speed and t is the time for receiving the echo.

A. Case I: Trajectory Tracking

Consider the kinematic model and the dynamic model of the mobile robot given by (1) and (2), respectively. Assume that the admissible configuration set $\mathcal{P}_a$ is defined by

$$\mathcal{P}_a = \left\{ (x, y) \middle| \begin{array}{l} -0.2 \le x \le 2.9, \ -0.25 \le y \le 1.75 \\ y \in [-0.25, 0.2] \cup [1.2, 1.75] \quad \text{if } x \in [0.7, 2.4] \\ x \in [-0.2, 0.7] \cup [2.4, 2.9] \quad \text{if } y \in [0.2, 1.2] \end{array} \right\} \tag{19}$$

and the reference trajectory is a straight line given by

$$p_d(t) = [x_d(t), y_d(t)]^T = [0.067t, 0.044t]^T. \tag{20}$$

This models the task in which the human user is restricted to drive the robot from its initial position $(0, 0)$ to the final position $(3, 2)$ along a straight line with a constant speed of 0.08 m/s. Note that the desired trajectory is not always feasible, i.e., $\exists t > 0$ such that $p_d(t)) \notin \mathcal{P}_a$.

The simulation results are shown in Figs. 7–10. Fig. 7 demonstrates that the (x, y) trajectory of the h-closed-loop system go through the nonadmissible region (the gray shaded rectangle), while that of the s-closed-loop system move along the boundary of $\mathcal{P}_a$ until the reference trajectory becomes feasible. It also shows that the configuration of the robot without shared control leaves $\mathcal{P}_a$ for a second time after 38 s as the red dashed-dotted and the yellow solid line indicate,

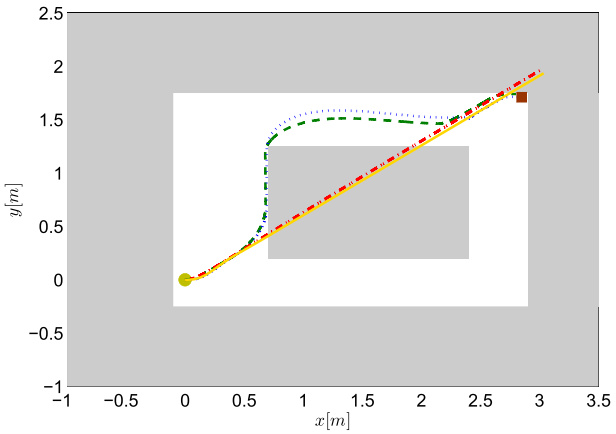

Fig. 7. (x, y) trajectories of the system for the set $\mathcal{P}_a$ given by (19): h-closed-loop (red dashed-dotted line) and s-closed-loop (green dashed line) for system (1), h-closed-loop (yellow solid line) and s-closed-loop (blue dotted line) for system (2). Round mark: the initial position of the robot. Square mark: the final position of the robot with shared control.

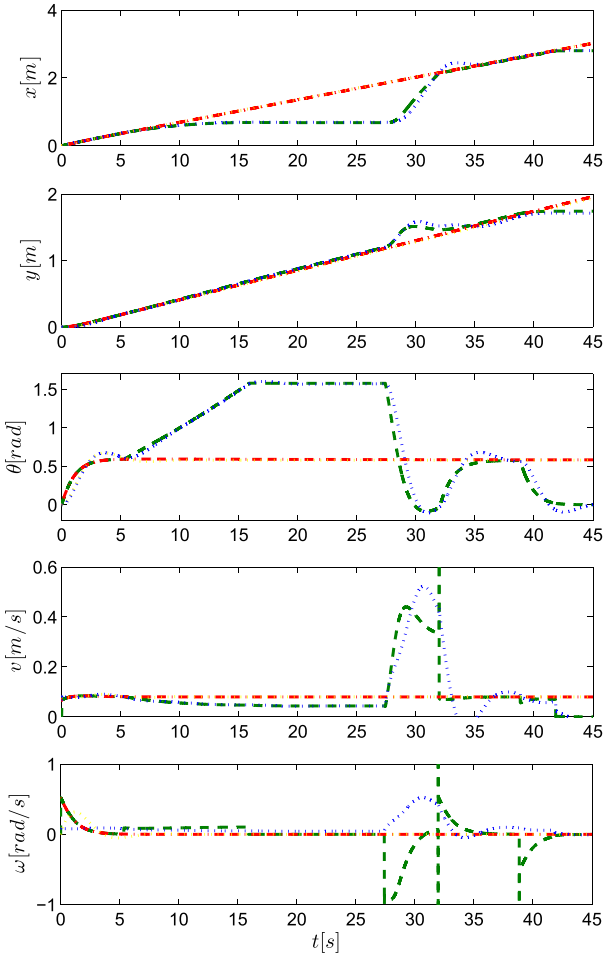

Fig. 8. Time histories of the variables x, y, θ, v, and ω for the system with set $\mathcal{P}_a$ given by (19): h-closed-loop (red dashed-dotted lines) and s-closed-loop (green dashed lines) for system (1), h-closed-loop (yellow solid lines) and s-closed-loop (blue dotted lines) for system (2).

while the robot with shared control stops at the boundary of the admissible set. Figs. 8 and 9 show the time histories of the states and inputs of the h-closed-loop system and

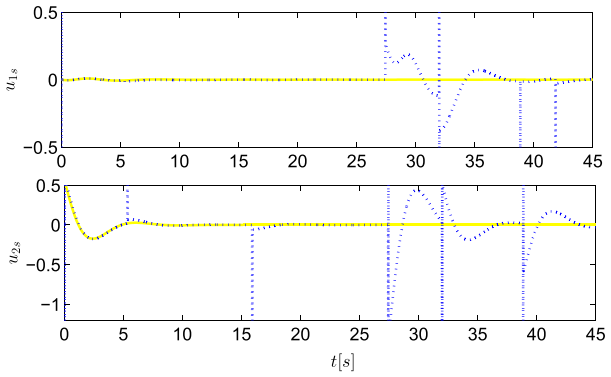

Fig. 9. Time histories of the inputs u_1 and u_2 for system (2) with set $\mathcal{P}_a$ given by (19): h-closed-loop (yellow solid lines) and s-closed-loop (blue dotted lines).

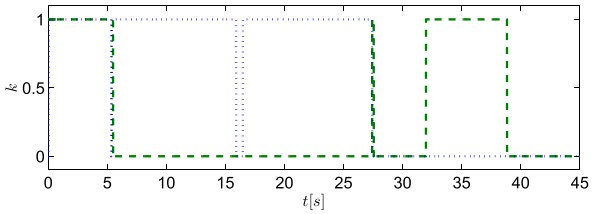

Fig. 10. Time histories of the sharing function k for systems (1) (green dashed line) and (2) (blue dotted line) with the set $\mathcal{P}_a$ given by (19).

s-closed-loop system. The functions $v(t)$ and $\omega(t)$ for system (2) are smoother than those for system (1) as they are system states rather than control inputs in the dynamic model of the mobile robot. Due to the discontinuity of d_r caused by the concavity of $\mathcal{P}_a$ and the fact that v and ω change more gently for the dynamic model of the robot, the error between the configuration of system (2) and its reference needs more time to converge to zero. Fig. 10 indicates that the feedback control is active for both systems (1) and (2) at 5.5 s as k changes its value to 0. However, the control authority for system (2) is passed to the human operator after a short period when the angular velocity of the robot is corrected by the feedback controller. In addition, due to the concavity of the feasible set $\mathcal{P}_a$, the robot needs to change its forward direction quickly to track the reference trajectory when $t \approx 16$ s. The feedback controller is active for less than 1 s to adjust the forward velocity and the angular velocity of the robot. Yet, the situation is different for system (1). The control authority is hold by the feedback controller until the robot has left the obstacle, because the human has direct control on the velocities.

The experiment has been performed in a rectangular room with a table in it. Therefore, the admissible configuration region can be described as

$$\mathcal{P}_a = \left\{ (x, y) \left| \begin{array}{l} -0.5 \le x \le 3, \ -0.5 \le y \le 2 \\ y \in [0, 0.2] \cup [0.8, 2] \quad \text{if } x \in [1, 2.5] \\ x \in [0, 1] \cup [2.5, 4.5] \quad \text{if } y \in [0.2, 0.8] \end{array} \right. \right\} \tag{21}$$

where (x, y) refers to every point of the robot. In other words, all the points of the robot should be located in the set $\mathcal{P}_a$ given by (21). Note that this set is equivalent to that described by (19) since (x, y) in (19) refers to the center of the robot's front wheels.

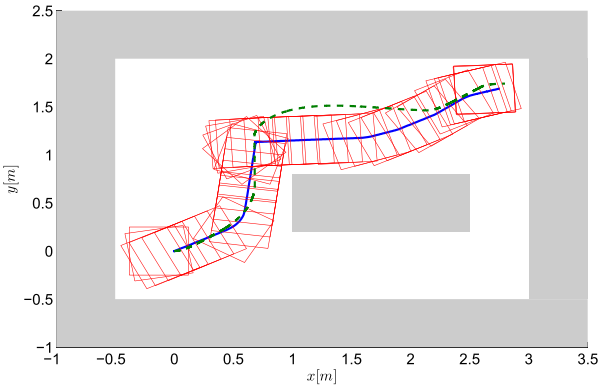

Fig. 11. Virtual path (green dashed line) generated in the simulation and the experimental path (blue solid line) of the mobile robot with the shared control for the set $\mathcal{P}_a$ given by (21).

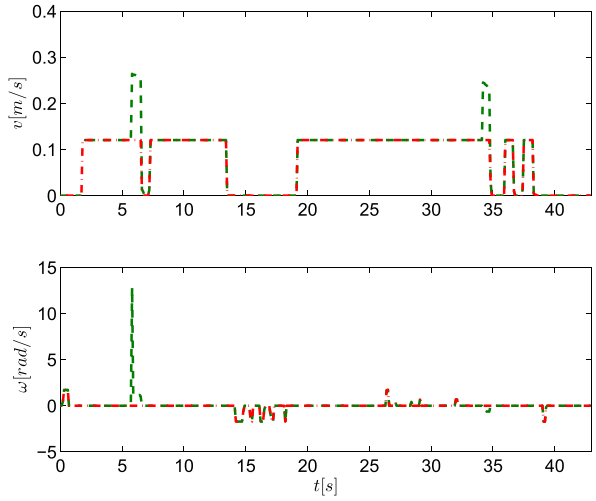

Fig. 12. Measured time histories of the inputs v and ω for the h-closed-loop system (red dashed-dotted lines) and the s-closed-loop system (green dashed lines).

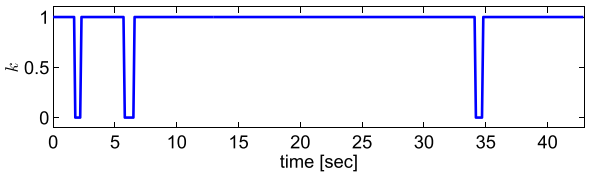

Fig. 13. Time history of the sharing function k during the experiment.

In the experiments, the linear velocity v and the angular velocity ω of the car can be controlled directly by changing the left-wheel speed v_L and the right-wheel speed v_R as

$$v = \frac{v_R + v_L}{2}, \quad \omega = \frac{v_R - v_L}{l}$$

where l is the length between the left-wheel and the right-wheel, which equals 0.5 m in the experiment. Therefore, the shared-control algorithm developed in Section III can be applied to control the robot.

Figs. 11–13 show the experimental results. Compared with the simulation results, we note that there are slight differences,

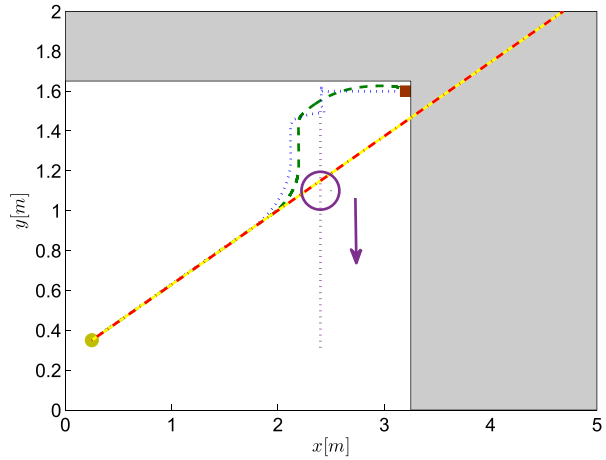

Fig. 14. (x, y) trajectories of the system for the set $\mathcal{P}_a$ given by (22): h-closed-loop (red dashed-dotted line) and s-closed-loop (green dashed line) for system (1), h-closed-loop (yellow solid line) and s-closed-loop (blue dotted line) for system (2). Round mark: the initial position of the robot. Square mark: the final position of the robot with shared control. Purple circle: the moving obstacle. Purple dotted curve: trajectory of the moving obstacle.

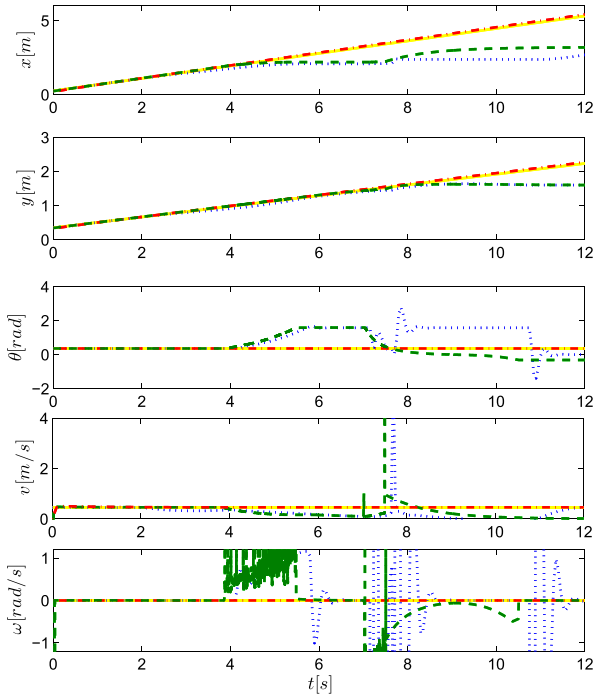

Fig. 15. Time histories of the variables x, y, θ, v, and ω for the system with set $\mathcal{P}_a$ given by (22): h-closed-loop (red dashed-dotted lines) and s-closed-loop (green dashed lines) for system (1), h-closed-loop (yellow solid lines) and s-closed-loop (blue dotted lines) for system (2).

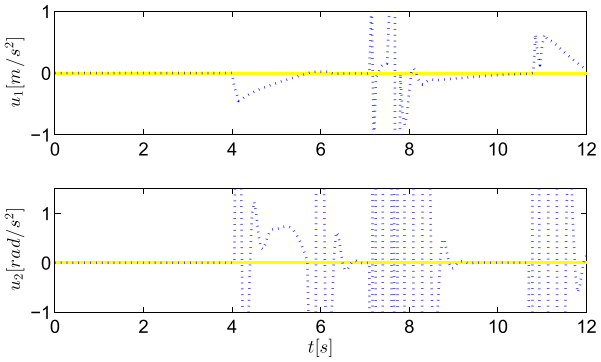

Fig. 16. Time histories of the inputs u_1 and u_2 for system (2) with set $\mathcal{P}_a$ given by (22): h-closed-loop (yellow solid lines) and s-closed-loop (blue dotted lines).

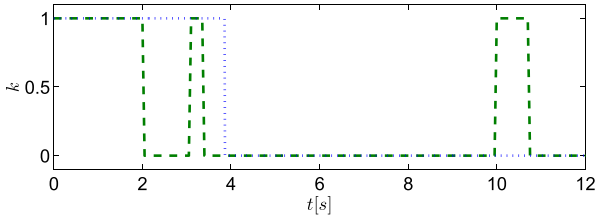

Fig. 17. Time history of the sharing function k for system (1) (green dashed line) and (2) (blue dotted line) with the set $\mathcal{P}_a$ given by (22).

because in the simulation, we assume that the h-control is a controller making the robot moving toward the target point following a straight line and at a constant speed, while in the experiment, this is done by the operator's intuition which is slightly different from the h-control in the simulation. Fig. 13 shows that the time period when $u_s = u_f$ is shorter than the simulation results for system (1) illustrated in Fig. 10. This is because in the experiment, the human operator has noticed that he/she has to change the direction of the robot to avoid collisions after feedback from the signal k. In addition, the average velocity in the experiment (approximately 0.12 m/s) is larger than that in the simulation (approximately 0.08 m/s) due to frictions.

B. Case II: Moving Obstacles

The second case study deals with moving obstacles. Consider the kinematic model and the dynamic model of the mobile robot given by (1) and (2), respectively. Assume that the robot is able to move within a rectangular room defined by

$$\mathcal{P}_a = \{(x, y) | x \leq 3.25,\ \ y \leq 1.65\} \tag{22}$$

and there is moving obstacle, the shape of which is a circle with a radius of 0.2 m, going along a straight line from $(2.4, 1.5)$ to $(2.4, 0.3)$ with a forward speed of $v = 0.1$ m/s. Suppose the reference trajectory is a straight line described by

$$p_d(t) = [x_d(t), y_d(t)]^T = [0.25 + 0.43t, 0.35 + 0.16t]^T. \tag{23}$$

This models the task in which the human is asked to drive the robot from the initial position $(0.25, 0.35)$ to its final position $(4.7, 2)$ along a straight line with the speed $v = 0.45$ m/s. Note that the final target position is unfeasible, i.e., $(4.7, 2) \notin \mathcal{P}_a$.

The simulation results are displayed in Figs. 14–17. From Fig. 14, it is clear that the mobile robot with the shared control changes its direction to avoid hitting the moving obstacle represented by the purple circle. Even though the purple circle is moving, Fig. 14 only shows its position when it starts to affect the robot (i.e., when it is close to the robot and force

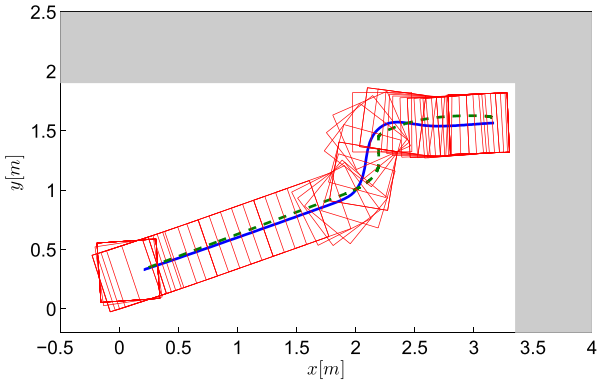

Fig. 18. Virtual path (green dashed line) and the experimental path (blue solid line) of the mobile robot with the shared control for the set $\mathcal{P}_a$ given by (24).

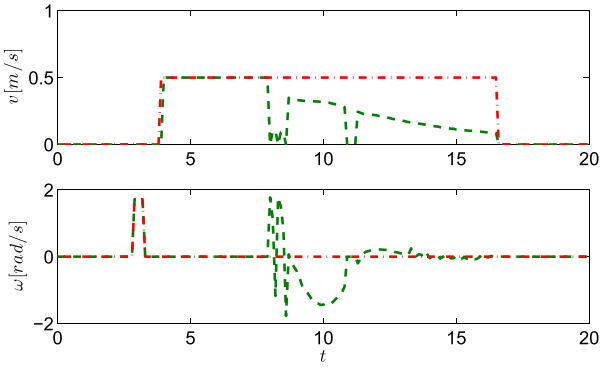

Fig. 19. Measured time histories of the inputs v and ω for the h-closed-loop system (red dashed-dotted lines) and the s-closed-loop system (green dashed lines).

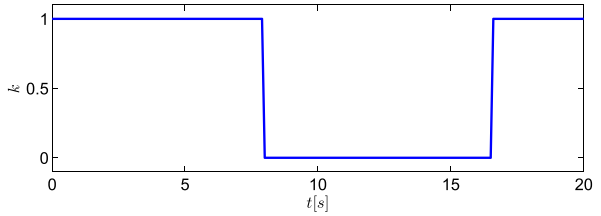

Fig. 20. Time history of the sharing function k during the experiment.

the feedback-controller to be active). Figs. 15 and 16 show the time histories of the states and inputs of the h-closed-loop systems and the s-closed-loop systems. The blue time histories in Fig. 15 are smoother than the green time histories, especially for the function $v(t)$ and $\omega(t)$, because v and ω are system states rather than input signals in system (2). In addition, the chattering in the control input ω illustrated in the bottom plot in Fig. 15 is mainly caused by the moving obstacle and can be reduced by predicting the trajectory of the moving obstacle. Due to the unfeasibility of the final position, the robot with the shared control for both systems (1) and (2) stops at the boundary of the rectangular room. When $t > 11$ s, even if the human input u_h is nonzero, the shared-control input of the system is $u_s = 0$. Fig. 17 shows how the control authority is allocated between the human operator ($k = 1$) and the feedback controller ($k = 0$).

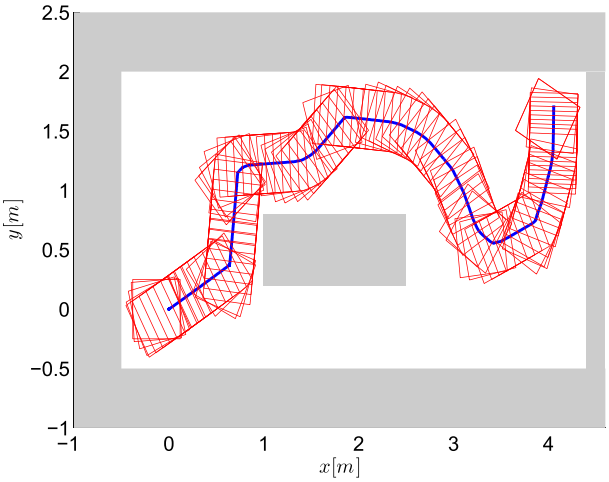

Fig. 21. Paths of the mobile robot with the shared control for the set $\mathcal{P}_a$ (white area) given by (25).

The experiment has been done in a rectangular room described by

$$\mathcal{P}_a = \{(x, y) | x \leq 3.35,\ \ y \leq 1.9\} \tag{24}$$

where (x, y) refers to every point of the robot. During the experiment, a person is walking in the room with a speed of 0.1 m/s. Therefore, the experimental setting is the same as that given in the simulation part. The experimental results are demonstrated in Figs. 18–20. Fig. 18 shows that the robot with the shared controller successfully avoids the collision with the pedestrian and walls, which meets our expectations and proves the effectiveness of the shared-control law. Fig. 19 shows that the shared-control input v_s drops to 0 rather than decline gently according to its previous trend at $t = 16$ s because the human input u_h falls to 0 suddenly. Fig. 20 illustrates the time period in which the feedback controller is active in the experiment.

C. Case III: Free Driving

The third case study is motivated by application to a toy car: the car is driven by the operator while away from dangerous situations. In real applications, it is usually difficult to define the reference trajectory due to the unknown task and uncertainties of the environment. Therefore, we need to predict the desired trajectory based on the online measurement of the human inputs and the states.

In the experiment, the human operator has been asked to drive the robot freely without tracking any trajectory in a rectangular room with a table in it. The room can be described as

$$\mathcal{P}_a = \left\{ (x, y) \left| \begin{array}{ll} -0.5 \leq x \leq 4.4, & -0.5 \leq y \leq 2 \\ y \in [-0.5, 0.2] \cup [0.8, 2] & \text{if } x \in [1, 2.5] \\ x \in [-0.5, 1] \cup [2.5, 4.4] & \text{if } y \in [0.2, 0.8] \end{array} \right. \right\}. \tag{25}$$

Fig. 21 shows the (x, y) trajectory of the robot with the shared controller, while Fig. 22 illustrates how the inputs of the h-closed-loop system and the s-closed-loop system vary with time. In addition, Fig. 23 indicates how the control authority is shared between the human operator and the

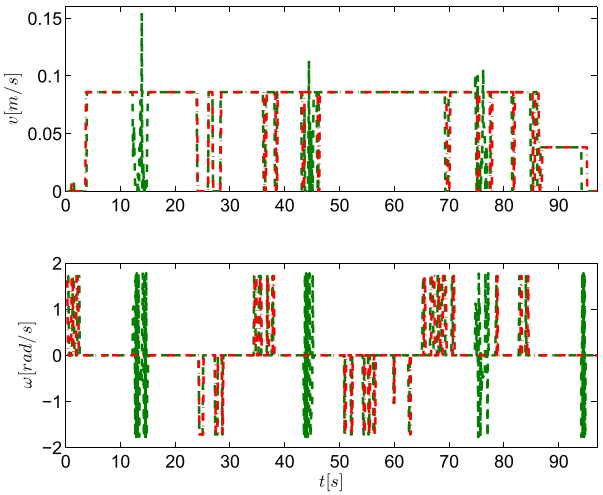

Fig. 22. Measured time histories of the inputs v and ω for the h-closed-loop system (red dashed-dotted lines) and the s-closed-loop system (green dashed lines).

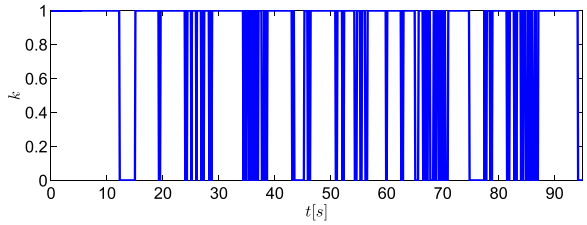

Fig. 23. Time history of the sharing function k during the experiment.

feedback controller. The experiment demonstrates the fact that the robot with the shared-control algorithm moves inside of the room and does not hit any obstacle (including both the table and the walls). Before any collision happens, the shared controller would drive the robot moving along the obstacle until the states of the s-closed-loop system enter the safe region $\mathcal{R}_s$, where the human operator has the control authority. Fig. 22 shows that v_s drops down to zero before v_h becomes zero, which indicates that the robot stops in front of the wall even if the human input is nonzero when it is close to the wall and tends to hit the wall.

VI. Conclusion

We have developed a solution to the shared-control problem for the kinematic model and the dynamic model of a mobile robot without the knowledge of its absolute position. A hysteresis switch is built to integrate the human input and the feedback control input. The shared-control algorithm is developed for general admissible configuration sets with the assumption that d_d is continuous. Both the simulation results and the experimental results with a Pioneer 3-AT robot show the effectiveness of the shared-control law. Future research will focus on the shared-control design for cars and multiagent systems.

References

[1] S. G. Tzafestas, *Introduction to Mobile Robot Control*. Amsterdam, The Netherlands: Elsevier, 2014.

[2] T. Carlson and Y. Demiris, "Collaborative control for a robotic wheelchair: Evaluation of performance, attention, and workload," *IEEE Trans. Syst., Man, Cybern. B, Cybern.*, vol. 42, no. 3, pp. 879–888, Jun. 2012.

[3] T. Rofer and A. Lankenau, "Ensuring safe obstacle avoidance in a shared-control system," in *Proc. 7th IEEE Int. Conf. Emerg. Technol. Factory Autom.*, vol. 1. Barcelona, Spain, Oct. 1999, pp. 1405–1414.

[4] J.-H. Kim, J.-C. Lee, and Y.-R. Choi, "LAROB: Laser-guided underwater mobile robot for reactor vessel inspection," *IEEE/ASME Trans. Mechatronics*, vol. 19, no. 4, pp. 1216–1225, Aug. 2013.

[5] H. Rezaee and F. Abdollahi, "A decentralized cooperative control scheme with obstacle avoidance for a team of mobile robots," *IEEE Trans. Ind. Electron.*, vol. 61, no. 1, pp. 347–354, Jan. 2014.

[6] M. Seder, K. Maček, and I. Petrović, "An integrated approach to real-time mobile robot control in partially known indoor environments," in *Proc. 31st Annu. Conf. IEEE Ind. Electron. Soc.*, Nov. 2005, pp. 1785–1790.

[7] K. Kanjanawanishkul and A. Zell, "Path following for an omnidirectional mobile robot based on model predictive control," in *Proc. IEEE Int. Conf. Robot. Autom.*, May 2009, pp. 3341–3346.

[8] A. Tahirovic and G. A. Magnani, "General framework for mobile robot navigation using passivity-based MPC," *IEEE Trans. Autom. Control*, vol. 56, no. 1, pp. 184–190, Jan. 2010.

[9] G. A. dos Reis, A. G. Siqueira, and M. H. Terra, "Nonlinear $\mathcal{H}_\infty$ control via quasi-LPV representation and game theory for wheeled mobile robots," in *Proc. 13th Medit. Conf. Control Autom.*, Limassol, Cyprus, 2005, pp. 686–691.

[10] J.-X. Xu, Z.-Q. Guo, and T. H. Lee, "Design and implementation of integral sliding-mode control on an underactuated two-wheeled mobile robot," *IEEE Trans. Ind. Electron.*, vol. 61, no. 7, pp. 3671–3681, Jul. 2013.

[11] S. X. Yang, A. Zhu, G. Yuan, and M. Q.-H. Meng, "A bioinspired neurodynamics-based approach to tracking control of mobile robots," *IEEE Trans. Ind. Electron.*, vol. 59, no. 8, pp. 3211–3220, Aug. 2011.

[12] Z.-G. Hou, A.-M. Zou, L. Cheng, and M. Tan, "Adaptive control of an electrically driven nonholonomic mobile robot via backstepping and fuzzy approach," *IEEE Trans. Control Syst. Technol.*, vol. 17, no. 4, pp. 803–815, Jul. 2009.

[13] R.-J. Wai and Y.-W. Lin, "Adaptive moving-target tracking control of a vision-based mobile robot via a dynamic Petri recurrent fuzzy neural network," *IEEE Trans. Fuzzy Syst.*, vol. 21, no. 4, pp. 688–701, Aug. 2012.

[14] L. Leottau and M. Melgarejo, "A simple approach for designing a type-2 fuzzy controller for a mobile robot application," in *Proc. Annu. Meeting North Amer. Fuzzy Inf. Process. Soc.*, 2010, pp. 1–6.

[15] C.-F. Juang and C.-H. Hsu, "Reinforcement ant optimized fuzzy controller for mobile-robot wall-following control," *IEEE Trans. Ind. Electron.*, vol. 56, no. 10, pp. 3931–3940, Oct. 2009.

[16] C. Samson, "Control of chained systems application to path following and time-varying point-stabilization of mobile robots," *IEEE Trans. Autom. Control*, vol. 40, no. 1, pp. 64–77, Jan. 1995.

[17] Z. Qu, J. Wang, C. E. Plaisted, and R. A. Hull, "Global-stabilizing near-optimal control design for nonholonomic chained systems," *IEEE Trans. Autom. Control*, vol. 51, no. 9, pp. 1440–1456, Sep. 2006.

[18] H. Fujimoto, S. Yamakawa, and Y. Funahashi, "Switching control of chained systems based on time-state control form," in *Proc. 26th Annu. Conf. IEEE Ind. Electron. Soc.*, vol. 2. Oct. 2000, pp. 1105–1110.

[19] J. Jiang and A. Astoli, "Shared-control for fully actuated linear mechanical systems," in *Proc. IEEE Conf. Decision Control*, Florence, Italy, Dec. 2013, pp. 4699–4704.

[20] N. Uchiyama, T. Hashimoto, S. Sano, and S. Takagi, "Model-reference control approach to obstacle avoidance for a human-operated mobile robot," *IEEE Trans. Ind. Electron.*, vol. 56, no. 10, pp. 3892–3896, Oct. 2009.

[21] L. Tonin, R. Leeb, M. Tavella, S. Perdikis, and J. R. del Millan, "The role of shared-control in BCI-based telepresence," in *Proc. IEEE Int. Conf. Syst. Man Cybern.*, Oct. 2010, pp. 1462–1466.

[22] C. Masone, A. Franchi, H. H. Bulthoff, and P. R. Giordano, "Interactive planning of persistent trajectories for human-assisted navigation of mobile robots," in *Proc. IEEE/RSJ Int. Conf. Intell. Robots Syst.*, Vilamoura, Portugal, Oct. 2012, pp. 2641–2648.

[23] H. Rifaï, M.-D. Hua, T. Hamel, and P. Morin, "Haptic-based bilateral teleoperation of underactuated unmanned aerial vehicles," in *Proc. 18th IFAC World Congr.*, Milan, Italy, 2011, pp. 13782–13788.

[24] C. Masone, A. Franchi, H. H. Bülthoff, and P. R. Giordano, "Shared trajectory planning for human-in-the-loop navigation of mobile robots in cluttered environments," in *Proc. 5th Int. Workshop Human-Friendly Robot.*, 2012.

[25] C. Masone, P. R. Giordano, H. H. Bülthoff, and A. Franchi, "Semi-autonomous trajectory generation for mobile robots with integral haptic shared control," in *Proc. IEEE Int. Conf. Robot. Autom.*, Hong Kong, May/Jun. 2014, pp. 6468–6475.
[26] P. Stegagno, M. Basile, H. H. Bülthoff, and A. Franchi, "A semi-autonomous UAV platform for indoor remote operation with visual and haptic feedback," in *Proc. IEEE Int. Conf. Robot. Autom.*, Hong Kong, May/Jun. 2014, pp. 3862–3869.
[27] J. Jiang and A. Astolfi, "Shared-control for the kinematic model of a mobile robot," in *Proc. IEEE 53rd Annu. Conf. Decision Control*, Los Angeles, CA, USA, Dec. 2014, pp. 62–67.
[28] C. Prieur, "Uniting local and global controllers with robustness to vanishing noise," *Math. Control Signals Syst.*, vol. 14, no. 2, pp. 143–172, 2001.
[29] D. Liberzon, *Switching in Systems and Control*. Boston, MA, USA: Birkhäuser, 2003.

Jingjing Jiang was born in China in 1988. She received the B.Eng. degrees in electrical and electronic engineering from the University of Birmingham, U.K., and the Harbin Institute of Technology, China, in 2010, and the M.Sc. Degree in control systems with the Department Prize for Outstanding Achievement from Imperial College London, London, U.K., in 2011, where she is currently pursuing the Ph.D. degree.

Her current research interests include control design of systems with constraints, human-in-the-loop, and driver assistance control.

Pierluigi Di Franco was born in Potenza, Italy, in 1988. He received the bachelor's and master's (*cum laude*) degrees in control engineering from the University of Rome Tor Vergata, Rome, Italy, in 2012 and 2015, respectively. He is currently pursing the Ph.D. degree with the Control and Power Group, Imperial College of London, London, U.K.

He was a Visiting Student with the Electrical and Electronic Engineering Department, Imperial College of London, from 2013 to 2014 and in 2015, and the Engineering and Architecture Department, University of Trieste, Trieste, Italy, in 2015. His current research interests include control of nonlinear differential-algebraic systems and applications.

Alessandro Astolfi (F'09) was born in Rome, Italy. He received the B.Eng. degree in electrical engineering from the University of Rome, Rome, in 1991, the M.Sc. and Ph.D. (Hons.) degrees from ETH Zurich, Zürich, Switzerland, in 1995, and the Ph.D. degree from the University of Rome, in 1996.

He has been with the Electrical and Electronic Engineering Department, Imperial College London, London, U.K., since 1996, where he is currently a Professor of Nonlinear Control Theory and the Head of the Control and Power Group. He was an Associate Professor with the Politecnico of Milano, Milan, Italy, from 1998 to 2003. He has also been a Professor with the University of Rome Tor Vergata, Rome, since 2005. His current research interests include control theory and applications, with special emphasis for the problems of discontinuous stabilization, robust and adaptive control, observer design, and model reduction.

Dr. Astolfi, a Distinguished Member of the IEEE Control Systems Society (CSS), was a recipient of the IEEE CSS A. Ruberti Young Researcher Prize in 2007, and the IEEE CSS George S. Axelby Outstanding Paper Award in 2012.